Thermal Science and Engineering Progress 39 (2023) 101751

Contents lists available at ScienceDirect

Thermal Science and Engineering Progress

journal homepage: www.sciencedirect.com/journal/thermal-science-and-engineering-progress

# Optimization of the surface heating for a stationary cascade turbine blade in wet steam flow

Jalal Salimi [a], Ali Reza Teymourtash [a], Mohammad Reza Aghdasi [a], Esmail Lakzian [b,c,*]

[a] Department of Mechanical Engineering, Ferdowsi University of Mashhad, Mashhad, Iran
[b] Center of Computational Energy, Department of Mechanical Engineering, Hakim Sabzevari University, Sabzevar, Iran
[c] Department of Mechanical Engineering, Andong National University, Andong, South Korea

ARTICLE INFO

*Keywords:*
Surface heating
Nozzle efficiency
Entropy
Mean wetness
Mean momentum
Cost price

ABSTRACT

The purpose of this study is to obtain the optimal surface heating for a stationary cascade turbine blade in wet steam flow by a genetic algorithm. The numerical method is conducted by employing two-dimensional Navier–Stokes equations coupled with a $SSTk-\omega$ turbulence model. Nucleation and droplet growth equations are solved using the Eulerian-Eulerian approach. The numerical results show good agreement with well-established experiments. Nozzle efficiency (NE), integral of local entropy changes at the outlet (ILE), mean wetness at the outlet (MWO), mean momentum at the outlet (MMO), and cost price (CP) are objective functions. The ultimate purpose is to minimize the (ILE), (MWO), and (CP) and maximize the (NE) and (MMO) together. Since higher surface heating rates decrease MWO and MMO, while increasing ILE, CP, and NE based on optimization results, there is an optimum for the surface heating rate to gain the best performance of steam turbines. According to the numerical results, the optimum – is equal to 0.04467 ($\frac{kW}{cm^2}$). In the optimal case compared to the non-heat case, NE and MWO are improved 0.26% and 19.94%, respectively. In addition, the ILE and MMO are degraded 0.9%, 0.32%, respectively, and CP is estimated 0.0027 ($\frac{\$}{cm^2.h}$).

## 1. Introduction

In many industrial pieces of equipment, such as nozzles [1], steam turbine blades [2], and ejectors [3] are prone to the additional losses impact enforced by condensation. In this regard, some researchers investigated this phenomenon [4]. Wisniewski et al. [5] investigated the impact of condensation models on the simulation of condensation phenomena in wet steam transonic flow through a nozzle and the external flow around an airfoil. Zhang et al. [6] evaluated the relationship of two-phase heat transfer with the performance of the ejector in the condensing flow regime under the primary steam superheating condition. Wen et al. [7] investigated the impacts of four different turbulence models on the condensation behavior in transonic flows considering shock waves. Their results indicated that the $SSTk-\omega$ was a suitable model to predict the non-equilibrium condensation and shock waves in transonic flows. Zhang et al. [8] studied the impact of the impurities in steam on the non-equilibrium condensation phenomenon. They used sodium chloride (NaCl) to gain their goal because salt is a very common steam impurity. Their results showed that the attendance of salt particles decreased the outlet average liquid mass fraction and entropy generation.

There are several methods to measure a multiphase flow system. Walker et al. [9] reviewed different methods used to measure the wetness content. Salmani et al. [10] suggested a method to predict droplet radius and wetness fraction which was founded on Buckingham Pi-theorem. Results indicated that their technique was a useful method for simulating the real operation condition in wet steam devices.

A great number of researchers have used various methods to decrease the liquid mass fraction and droplet size in industrial equipment. Aghdasi et al. [11] proposed the optimum pitch to the axial chord for a stationary cascade turbine blade. Their results demonstrated that the wetness and average droplet radius were decreased in the optimal case. Hoseinzade et al. [12] obtained the optimum of the trailing edge rotation at the last stage of the steam turbine. Their results showed that, in the proposed case, the liquid mass fraction and average droplet radius were decreased. Kafaei et al. [13] injected hot steam in the turbine blade. In the optimal case, the wetness fraction was decreased. Dolatabadi et al. [14] utilized TOPSIS method to optimize the hot steam

* Corresponding author at: Center of Computational Energy, Department of Mechanical Engineering, Hakim Sabzevari University, Sabzevar, Iran.
*E-mail address:* e.lakzian@hsu.ac.ir (E. Lakzian).

https://doi.org/10.1016/j.tsep.2023.101751
Received 20 July 2022; Received in revised form 13 February 2023; Accepted 20 February 2023
Available online 24 February 2023

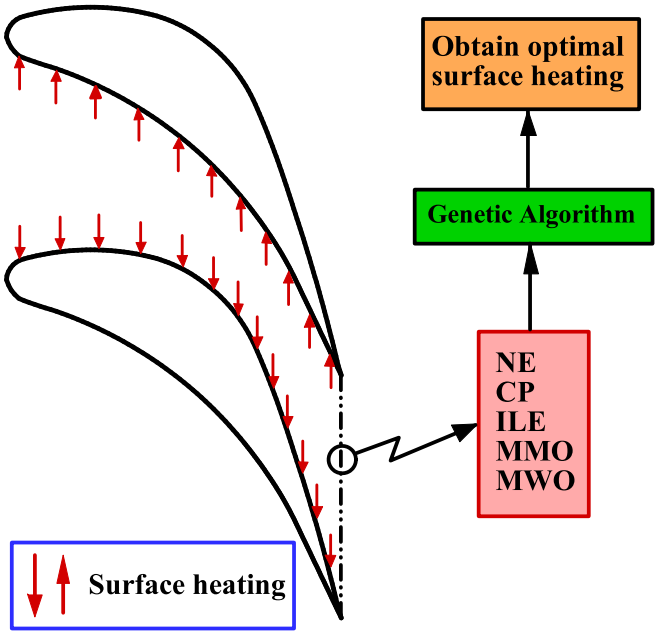


**Fig. 1.** The schematic of the cascade turbine blade and objective function.

injection for the nozzle. Their results indicated that the droplet radius, losses, and liquid mass fraction were decreased by applying an optimal injection. Dolatabadi et al. [15] used the suction method in the divergent section of the nozzle to dehumidify and increase power-saving. The wetness loss, power-saving, and erosion rate were their parameters.

A considerable number of researches have also been conducted on the volumetric heating impacts. Vatanmakan et al. [16] investigated the volumetric heating impacts on condensing steam flow in the turbine blade cascade. Their results illustrated that, by applying appropriate volumetric heating, the liquid mass fraction and entropy generation were decreased. Hosseini and Lakzian [17] proposed a novel technique based on entropy losses, economic cost, and wetness to optimize the volumetric heating for the turbine blade cascade. Hoseinzade et al. [18] applied volumetric heating to the converging section of the turbine blade. A genetic algorithm was used to obtain a suitable rate of volumetric heating.

Surface heating has also been investigated to reduce the adverse effects of liquid mass fraction in the low-pressure section of the steam turbine, ejector, and nozzle. Han et al. [19] designed an end-wall fence and heated it in a White cascade. Aerodynamic performance analysis, dehumidification performance, entropy generation, and enthalpy drop were investigated for different positions and heats of the end wall fence. Han et al. [20] studied the impacts of stator blade surface heating, rotor, and simultaneous heating on the condensation phenomenon. Their study showed that heating the surface of the stator blade can satisfactorily prevent vapor condensation. Han et al. [21] investigated surface heating in a steam turbine and analyzed wetness, entropy, enthalpy, and Mach number, and suggested the amount of surface heating accordingly. Jahani-Rahavard et al. [22] evaluated the effects of surface heating on ejector performance. Their results showed that surface heating decreased wetness. Han et al. [23] utilized surface heating for the dehumidification of Moses and Stein nozzles.

With the great effort of the aforementioned studies, no attempt has been done to optimize the surface heating for wet steam flow in turbine blade cascade. The innovation of this study is the optimization of surface heating with the use of the nozzle efficiency (NE), integral of local entropy changes at the outlet (ILE), mean wetness at the outlet (MWO), mean momentum at the outlet (MMO), and cost price (CP) and a genetic algorithm. In this regard, two-dimensional Navier–Stokes equations coupled with an SST k-ω turbulence model. Nucleation and droplet growth equations are conducted to simulate the viscous wet steam flow through the turbine blade cascade. Fig. 1 indicates the schematic of this study.

**Table 1**
Geometrical information for Bakhtar nozzle blade [24].

| Chord | Pitch | Axial chord | Inlet flow angle |
|---|---|---|---|
| 35.76 mm | 18.26 mm | 25.27 mm | $0^0$ |

**Table 2**
Boundary conditions of cascade turbine blade [25].

| | |
|---|---|
| $\mathbf{P}_{0_{in}}$ | 172 kPa |
| $\mathbf{T}_{0_{in}} = \mathbf{T}_s(\mathbf{P}_{0_{in}}) - 8$ | 380.66 K |
| $\mathbf{P}_{out} = 0.48\mathbf{P}_{0_{in}}$ | 82.56 kPa |

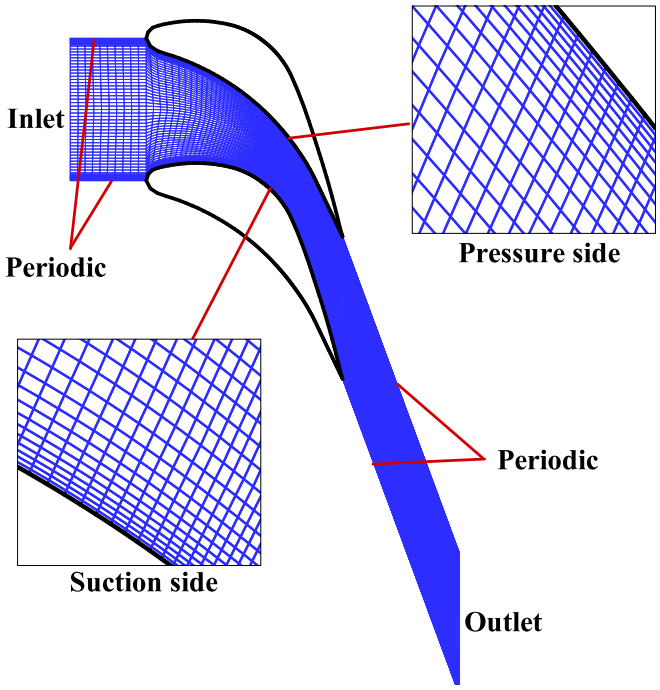


**Fig. 2.** Computational mesh and boundary conditions schematic.

## 2. Geometry and boundary conditions

In this paper, the Bakhtar nozzle blade [24] is utilized. Table 1 shows the information of this cascade.

Table 2 indicates the boundary conditions. Inlet and outlet conditions are pressure types. Besides, the blades are fixed with no-slip conditions. According to Fig. 2, the periodic boundary condition is used for the inlet and outlet of the passage.

## 3. Governing equations

Simulation of condensing steam flow is conducted by the Eulerian-Eulerian approach. Temperature (T), pressure (P), density (ρ), velocity (C), a liquid mass fraction (β), and number of liquid droplets per unit volume (η) are the unknown variables and calculated as follows:

- Energy equation is used to calculate the temperature.
- Equation of state is utilized to compute the pressure.
- Density is computed by the continuity equation.

- Velocities in two dimensions are calculated by solving the Navier-Stokes equations.
- Two additional transport equations are utilized to compute the droplet formation and mass transfer between the two phases.

### 3.1. Conservation equations

The steam flow assumed that viscous, turbulent, and compressible, and conservation equations of mass, momentum and energy in two-dimensional cartesian coordinates are defined as follows [26]:

$$\frac{\partial W}{\partial t}+\frac{\partial F}{\partial x}+\frac{\partial G}{\partial y}=\frac{\partial R}{\partial x}+\frac{\partial S}{\partial y} \tag{1}$$

Where $W$ displays the vector of the independent variable, $F$ and $G$ show non-viscous parameters, and $S$ and $R$ indicate viscous parameters as shown:

$$W=\begin{bmatrix}\rho\\ \rho C_x\\ \rho C_y\\ \rho e_0\end{bmatrix}, F=\begin{bmatrix}\rho C_x\\ P+\rho {C_x}^2\\ \rho C_x C_y\\ \rho C_x h_0\end{bmatrix}, G=\begin{bmatrix}\rho C_y\\ \rho C_y C_x\\ P+\rho {C_y}^2\\ \rho C_y h_0\end{bmatrix} S$$
$$=\begin{bmatrix}0\\ \tau_{xy}\\ \sigma_y\\ \sigma_y C_y+\tau_{xy}C_x+K_t\frac{\partial T}{\partial y}\end{bmatrix}, R=\begin{bmatrix}0\\ \sigma_x\\ \tau_{yx}\\ \sigma_x C_x+\tau_{yx}C_y+K_t\frac{\partial T}{\partial x}\end{bmatrix} \tag{2}$$

Where, $e_0$ and h0 show total energy and total enthalpy as follows:

$$e_0=e+\frac{C^2}{2} \tag{3}$$

$$h_0=h+\frac{C^2}{2} \tag{4}$$

$$C^2=C_x^2+C_y^2 \tag{5}$$

Furthermore, $\sigma_x$ and $\sigma_y$ represent normal stresses, and $\tau_{yx}$ and $\tau_{xy}$ show shear stresses as:

$$\sigma_x=-\frac{2}{3}\mu_{eff}\left(\frac{\partial C_x}{\partial x}+\frac{\partial C_y}{\partial y}\right)+2\mu_{eff}\frac{\partial C_x}{\partial x} \tag{6}$$

$$\sigma_y=-\frac{2}{3}\mu_{eff}\left(\frac{\partial C_x}{\partial x}+\frac{\partial C_y}{\partial y}\right)+2\mu_{eff}\frac{\partial C_y}{\partial y} \tag{7}$$

$$\tau_{xy}=\tau_{yx}=\mu_{eff}\left(\frac{\partial C_x}{\partial y}+\frac{\partial C_y}{\partial x}\right) \tag{8}$$

The summation of the turbulent viscosity and molecular viscosity is equal to effective viscosity ($\mu_{eff}$). Besides, two-phase density is calculated as follows:

$$\rho=\frac{\rho_v}{1-\beta} \tag{9}$$

Where $\beta$ is the liquid mass fraction. It is worth mentioning that two-phase mixture properties are computed as follows [27]:

$$\phi_{lv}=\phi_l\beta+(1-\beta)\phi_v$$

Where $\phi$ represents properties such as enthalpy and entropy. Besides, two equations are utilized to compute $\beta$ and $\eta$ as follows [28]:

$$\frac{\partial \rho\beta}{\partial t}+\frac{\partial}{\partial x_i}(\rho C_i\beta)=\Gamma \tag{11}$$

$$\frac{\partial \rho\eta}{\partial t}+\frac{\partial}{\partial x_i}(\rho C_i\eta)=\rho I \tag{12}$$

### 3.2. Nucleation and droplet growth equations

Phase change phenomenon in condensing steam flow includes nucleation and droplet growth processes. The Gibbs free energy change introduces the reversible work to form a single spherical droplet of radius r from a supersaturated vapor without the existence of external seeds [29]:

$$\Delta G=-m_r R T_v LnS+4\pi r^2\sigma \tag{13}$$

Where $S$ indicates the supersaturation ratio as follows [29]:

$$S=\left(\frac{P}{P_s(T_v)}\right) \tag{14}$$

Where $P$ shows vapor pressure and $P_s(T_v)$ represents saturation pressure at vapor temperature. Furthermore, $r^*$ indicates a critical radius. Besides, the critical Gibb's free energy change is expressed as $\Delta G^*$. It should be noted that $\Delta G^*$ and $r^*$ are calculated as follows [29]:

$$\Delta G^*=\frac{4}{3}\pi {r^*}^2 \tag{15}$$

$$r^*=\frac{2\sigma}{\rho_l R T_v LnS} \tag{16}$$

It is worth mentioning that the surface tension equation is as follows [30]:

$$\sigma_0(\mathrm{T})=235.8\left(1-\frac{\mathrm{T}}{647.3}\right)^{1.256}\left[1-0.625\left(1-\frac{\mathrm{T}}{647.3}\right)\right] \tag{17}$$

By using this model in the theory of the Gibbs surface tension, the error is increased. therefore, the Benson model [31] is utilized which expressed as follows:

$$\sigma=\sigma_0\left(1-\frac{\sqrt[3]{\frac{\rho_l}{m}}}{4.836\,r}\right) \tag{18}$$

According to the homogeneous condensation classical theory, the liquid droplet fetus formation rate is expressed as follows [29]:

$$I_{classic}=q_c\frac{\rho_v^2}{\rho_l}\sqrt{\frac{2\sigma}{\pi M_m^3}}.exp\left(-\frac{4\pi {r^*}^2\sigma}{3K_b T_v}\right) \tag{19}$$

A various number of corrections have been done to the homogeneous condensation classical theory. It should be noted that Kantrowitz corrections accuracy for non-isothermal impacts is satisfactory [29]:

$$I=\frac{1}{(1+\theta)}I_{classic} \tag{20}$$

Where $\theta$ shows the non-isothermal correction factor, and it is expressed as follows:

$$\theta=\frac{2(\gamma-1)}{(\gamma+1)}\left(\frac{h_{lv}}{RT}\right)\left(\frac{h_{lv}}{RT}-0.5\right) \tag{21}$$

Also,$\Gamma$ is the mass generation rate per unit volume as follows [29]:

$$\Gamma=\frac{4}{3}\pi\rho_l I {r^*}^3+4\pi\rho_l\eta\bar{r}^2\frac{\partial\bar{r}}{\partial t} \tag{22}$$

Where, $\frac{\partial\bar{r}}{\partial t}$ is the droplet growth rate:

$$\frac{\partial\bar{r}}{\partial t}=\frac{P}{h_{lv}\rho_l\sqrt{2\pi r T}}\left(\frac{\gamma+1}{2\gamma}\right)C_p(T_l-T_v) \tag{23}$$

Gyarmathy approximation is utilized for very small droplets ($r<1\mu m$) to compute droplet temperature $T_l$ as follows [29]:

$$T_l=T_s(p)-[T_s(p)-T_v]\frac{r^*}{r} \tag{24}$$

**Table 3**
Constant parameters of the state equation [32].

| $\tau_0$ | $\tau_1$ | $\tau_2$ | $\gamma_1$ | $\gamma_2$ | $b_1$ | $b_2$ | $b_3$ | $b_4$ | $b_5$ |
|---|---|---|---|---|---|---|---|---|---|
| 0.897 | 1500/T | T/647.286 | 10,000 | 11.16 | 0.0015 | $942 \times 10^{-3}$ | $-488.2 \times 10^{-6}$ | 1.722 | $1.5 \times 10^{-6}$ |

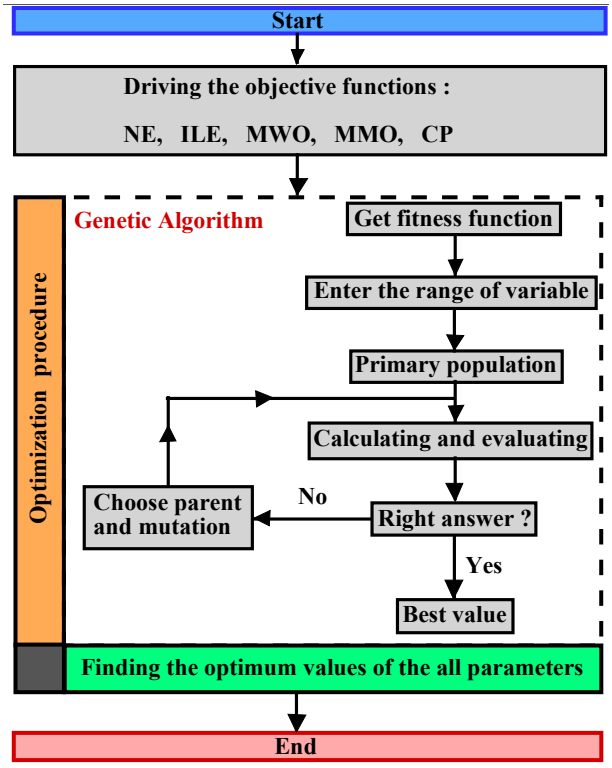


**Fig. 3.** Flowchart of the optimization process consists of GA [11].

### 3.3. State equation

To estimate the vapor properties, the state equation is employed as follows [32]:

$$\frac{P}{\rho_v RT} = 1 + B_2\rho_v + B_3{\rho_v}^2 \tag{25}$$

Where, $B_2$ and $B_3$ illustrate virial coefficients, which are expressed as follows:

$$B_2 = b_1\left(1+\frac{T}{\gamma_1}\right)^{-1} + b_2\exp(\tau_1)\left[1-\exp(-\tau_1)\right]^{\frac{5}{2}}\tau_1^{-\frac{1}{2}} + b_3\tau_1 \tag{26}$$

$$B_3 = b_4(\tau_2-\tau_0)\exp(-\gamma_2\tau_2) + b_5 \tag{27}$$

Besides, other constant parameters of the state equation are reported in Table 3.

### 3.4. Turbulence model

Various turbulent models have been stated to simulate the wet steam flow field in steam turbines. Menter [33] showed that the accuracy of the SST k −ω model for the whole domain is satisfactory. SST k −ω and k −ε models were compared by Rahimabadi et al. [34]. Their results illustrated that SST k −ω predicts the flow field of wet steam more accurately. The SST k −ω model is expressed as follows [33]:

$$\frac{\partial}{\partial t}(\rho k) + \frac{\partial}{\partial x_i}(\rho k C_i) = \frac{\partial}{\partial x_j}\left(\Gamma_k\frac{\partial k}{\partial x_j}\right) + G_K - Y_k + S_k \tag{28}$$

$$\frac{\partial}{\partial t}(\rho\omega) + \frac{\partial}{\partial x_i}(\rho\omega C_i) = \frac{\partial}{\partial x_j}\left(\Gamma_\omega\frac{\partial \omega}{\partial x_j}\right) + G_\omega - Y_\omega + D_\omega + S_\omega \tag{29}$$

### 3.5. Erosion equation

The presence of liquid droplets at the last stages of turbine blades causes erosion. Reduction of mechanical damages due to erosion is one of the essential issues in designing the turbine. The erosion rate is calculated by Lee et al. [35] with a model based on the droplet size, material hardness, collision rate of droplet flow, and collision velocity of the droplet. In this paper, an erosion rate ratio is defined as a dimensionless parameter as follows:

$$Err = \left(\frac{\beta}{\beta_{\text{non-heat case}}}\right)\left(\frac{\dot{m}}{\dot{m}_{\text{non-heat case}}}\right)\left(\frac{C}{C_{\text{non-heat case}}}\right)^{5.1}\left(\frac{r}{r_{\text{non-heat case}}}\right)^{4.5} \tag{30}$$

Here, $\beta$ shows the liquid mass fraction, $\dot{m}$ represents the mass flow rate, C displays the droplet velocity, and r indicates droplet size.

## 4. Multi objective optimization

In the present study, there are five objective functions, namely: nozzle efficiency (NE), mean wetness at the outlet (MWO), integral of local entropy changes at the outlet (ILE), mean momentum at the outlet (MMO), and cost price (CP). The final purpose is to minimize the (ILE), (MWO), and (CP) and maximize the (NE) and (MMO) together. Therefore, multi-objective optimization is utilized to gain the optimum surface heating. Fig. 3 illustrates the flowchart of multi-objective optimization. In this regard, the optimization toolbar of MATLAB software has been utilized. The optimization procedure consists four steps [11]:

- Objective functions are given to the algorithm as inputs value.
- For the aforementioned objective functions, 5 curves are fitted.
- The variations range in the surface heating is specified. Then genetic algorithm forms a population of this range.
- Based on the flowchart, the algorithm processes the results.

### 4.1. Defining objective functions

Nozzle efficiency (NE), mean wetness at the outlet (MWO), integral of local entropy changes at the outlet (ILE), mean momentum at the outlet (MMO), and cost price (CP) are objective functions of this study. Next, the objective functions are explained as:

$$NE = \frac{\dot{m}C^2}{\dot{m}_{dry}C_{dry}^2} = \frac{exit\ kinetic\ energy\ for\ wet\ flow\ condition}{exit\ kinetic\ energy\ for\ dry\ flow\ condition} \tag{31}$$

$$MWO = \frac{1}{A}\int_A (W)\ dA \tag{32}$$

$$ILE = \int_A \rho C s dA \tag{33}$$

$$MMO = \dot{m}C \tag{34}$$

The average global cost price of fuel is 0.06 ($\frac{\$}{\text{kW. h}}$). Thus, the generation cost price of surface heating by fuel is as follows [36]:

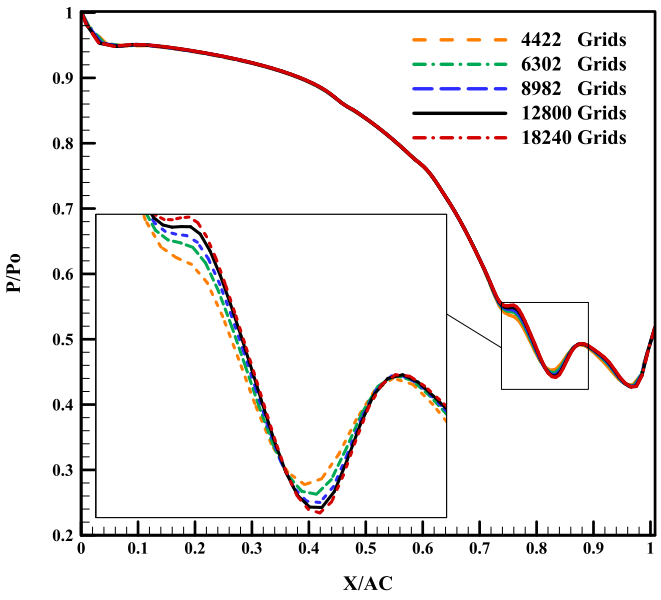


**Fig. 4.** Investigation of grid independency for the steam turbine.

$$CP(cost\ price)(\frac{\$}{cm^2.h}) = Q\left(\frac{kW}{cm^2}\right).0.06(\frac{\$}{kW.h}) \quad (35)$$

## 5. Numerical method

The stated numerical calculations were conducted with steady-state Reynolds-averaged Navier-Stokes equations. Therefore, the Eulerian-Eulerian approach is utilized to describe the two-phase flow properties. It is worth mentioning that an implicit density-based coupled solver is utilized in the modeling of the flow field. Besides, the calculation of the convective fluxes is based on the Roe method. Also, the SST k −ω turbulence model is selected for simulating the turbulent flow. The finite volume integration method is used to discretize the conservation equations of the vapor and liquid phases. Finally, reaching $10^{-6}$ for all dependent variables is the convergence criterion of this study.

### 5.1. Grid independence

Fig. 4 illustrates the static pressure distribution on the suction wall for various grid sizes. The quasi-orthogonal mesh is selected, and the grid size becomes smaller in critical regions. Based on this figure, the fourth grid (12800) illustrates the shocks very well. Thus, the 12,800 is selected as the optimum mesh size.

### 5.2. Validation

The experimental data of Bakhtar et al. [24] is used to validate the numerical manner. Fig. 5-a shows a comparison of the numerical and experimental data of the average droplet radius. There are some basic points in this figure. Bakhtar et al. [24] measured the droplet size on the mid line at the outlet of the blade, while in the present study, the average droplet radius is reported on the pressure side, suction side and center line, respectively just at the end of cascade; so the value of the droplet average radius for the experimental and numerical method are 0.057 and 0.042, respectively. Therefore, the error is equal to 25%. This amount of error can be seen in another previous study; for example, two cases are presented in the Table 4. It means that there is a possibility that a little laboratory study was done with an error in the measurement.

Fig. 5-b indicates the comparison of the numerical and experimental data of the pressure distribution on suction and pressure sides. Based on the Fig. 5-b, the flow pressure is decreased throughout the turbine blade cascade until the first shock (namely condensation shock) on the suction side happens. This shock occurs owing to the heat release between the two phases. Then flow expands until the second shock (first aerodynamic shock) happens. According to the back pressure at the end of the blade, the aerodynamic shock regulates the flow pressure. The position of this shock is at the end of the pressure side, and then it reflects

**Table 4**
Comparison of the numerical error in another previous study.

| | Numerical calculation | Error |
|---|---|---|
| [37] | 0.032 | 43% |
| [38] | 0.044 | 21% |
| Present study | 0.042 | 25% |

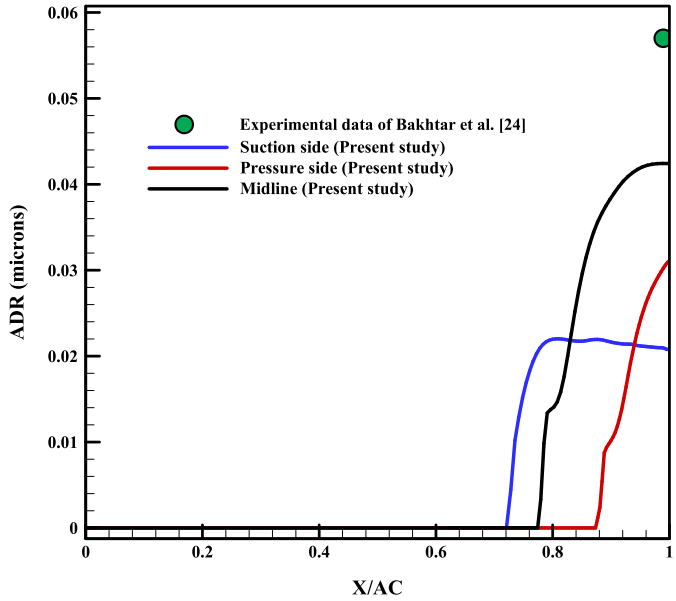


(a) ADR (Average droplet radius)

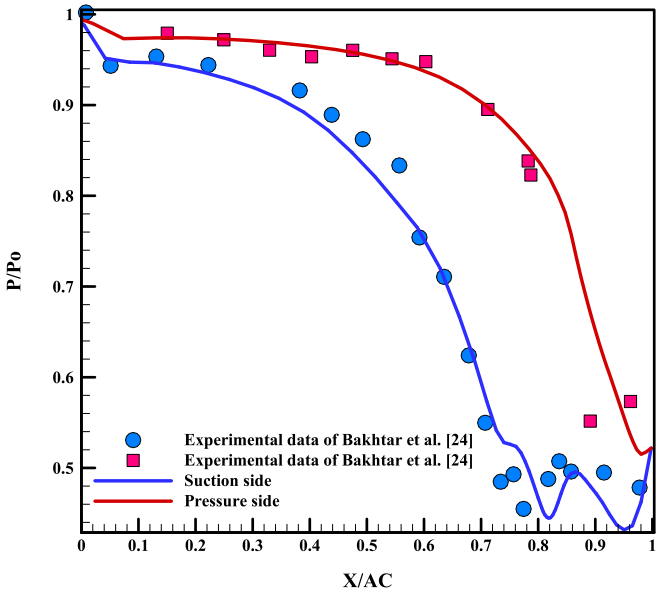


(b) Static pressure distributions

**Fig. 5.** Validation of numerical method with experimental data of Bakhtar et al. [24]. (a) illustration of ADR, and (b) static pressure distributions.

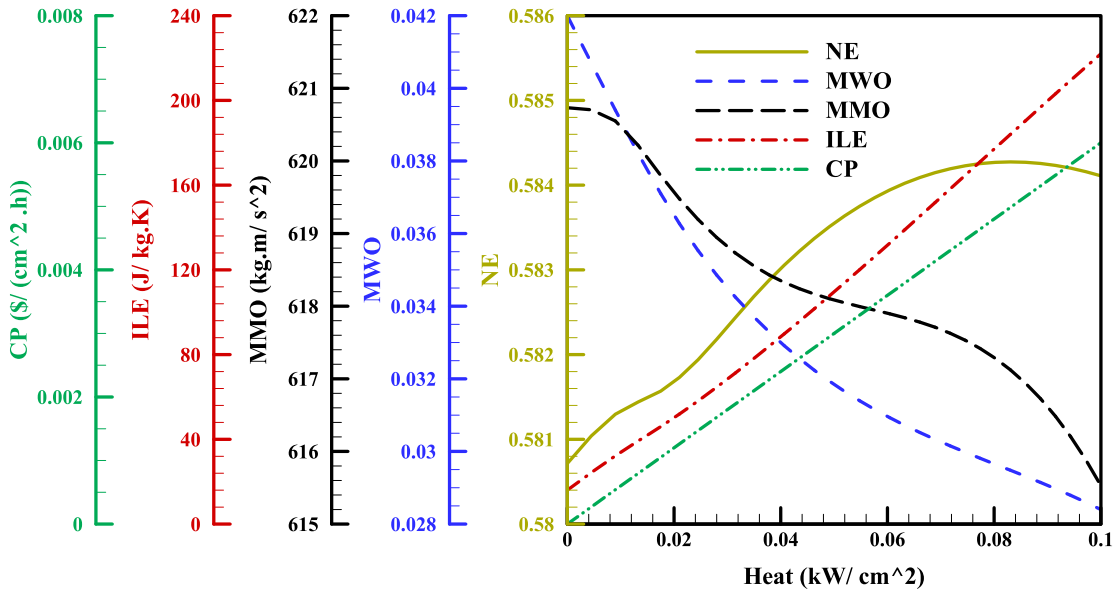


**Fig. 6.** The effect of surface heating on the parameters (NE. nozzle efficiency, MWO. mean wetness at the outlet, ILE. integral of local entropy changes at the outlet, MMO. mean momentum at the outlet, CP. cost price).

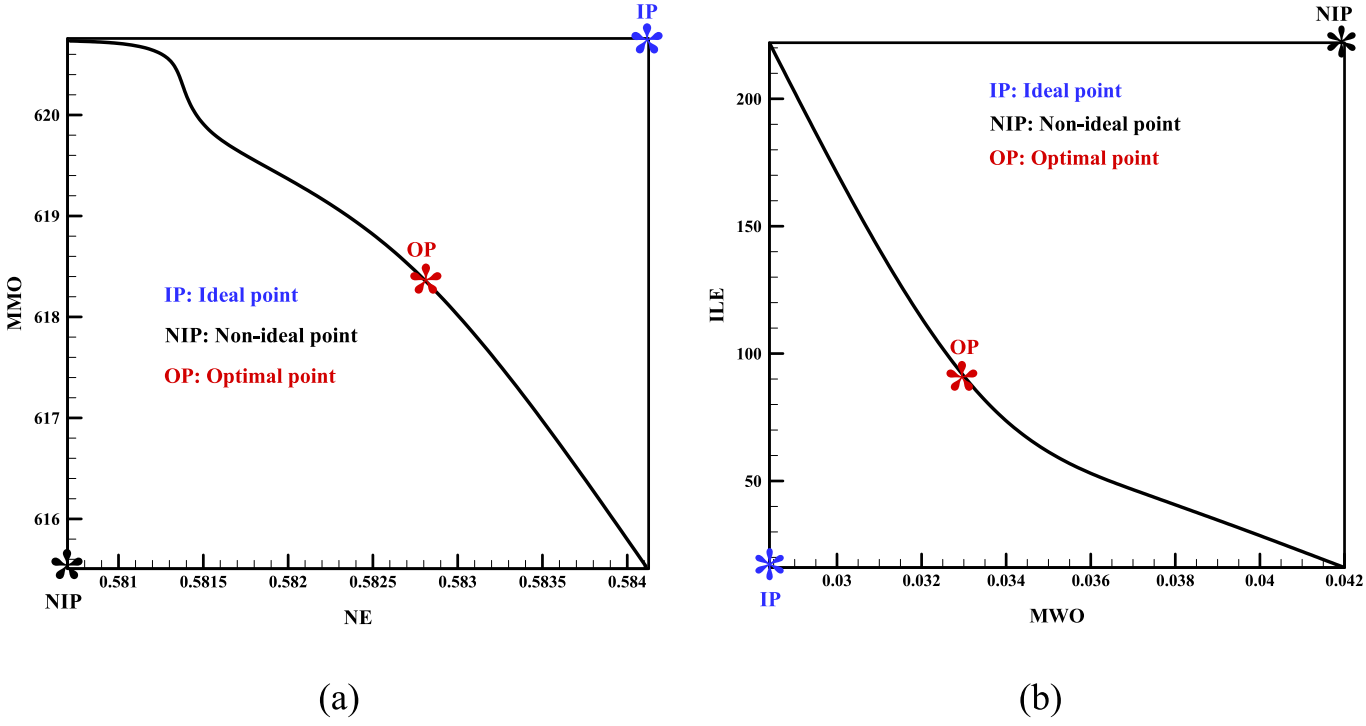


**Fig. 7.** The Pareto front of the multi-objective optimization as optimal solutions for objective functions; NE. nozzle efficiency, MWO. mean wetness at the outlet, ILE. integral of local entropy changes at the outlet, MMO. mean momentum at the outlet, CP. cost price.

on the suction wall. Based on the Fig. 5-b, the flow pressure is reduced further, and due to the reflection of aerodynamic shock, the second one happens at the end of the blade on the suction wall. The numerical results indicate a good consistency with experimental data.

## 6. The effect of surface heating on wet steam flow

The presence of the liquid phase in the last stages of the steam turbine leads to thermodynamic and mechanical losses. Surface heating is an effective method to decrease the losses in the wet steam turbine. In this section, the effects of surface heating on the parameters of the present study are evaluated. Fig. 6 shows the impacts of surface heating on the nozzle efficiency (NE), integral of local entropy changes at the outlet (ILE), mean wetness at the outlet (MWO), mean momentum at the outlet (MMO), and cost price (CP). As already shown in Fig. 6, NE, ILE, and CP are increased by applying surface heating. On the other hand, MWO and MMO are decreased by applying surface heating. It should be noted that increasing the NE and MMO is favorable. Besides, decreasing the MWO, CP, and ILE are desirable. Therefore, a genetic algorithm is used to find optimal surface heating.

**Table 5**
Comparison of the optimal and original amount of objective functions.

| NE | MWO | ILE | MMO | CP |
|---|---|---|---|---|
| Improved 0.26 % | Improved 19.94 % | Degraded 0.9 % | Degraded 0.32 % | Degraded 0.0027 ($\frac{\$}{cm^2.h}$) |

## 7. Optimization results

This study aims to optimize the surface heating in which the objective functions included the nozzle efficiency (NE), mean wetness at the outlet (MWO), integral of local entropy changes at the outlet (ILE), mean momentum at the outlet (MMO), and cost price (CP). Therefore, multi-objective optimization is used to optimize surface heating. One of the essential points in solving multi-objective optimization problems is to find the Pareto frontier. The Pareto frontier is plotted in terms of

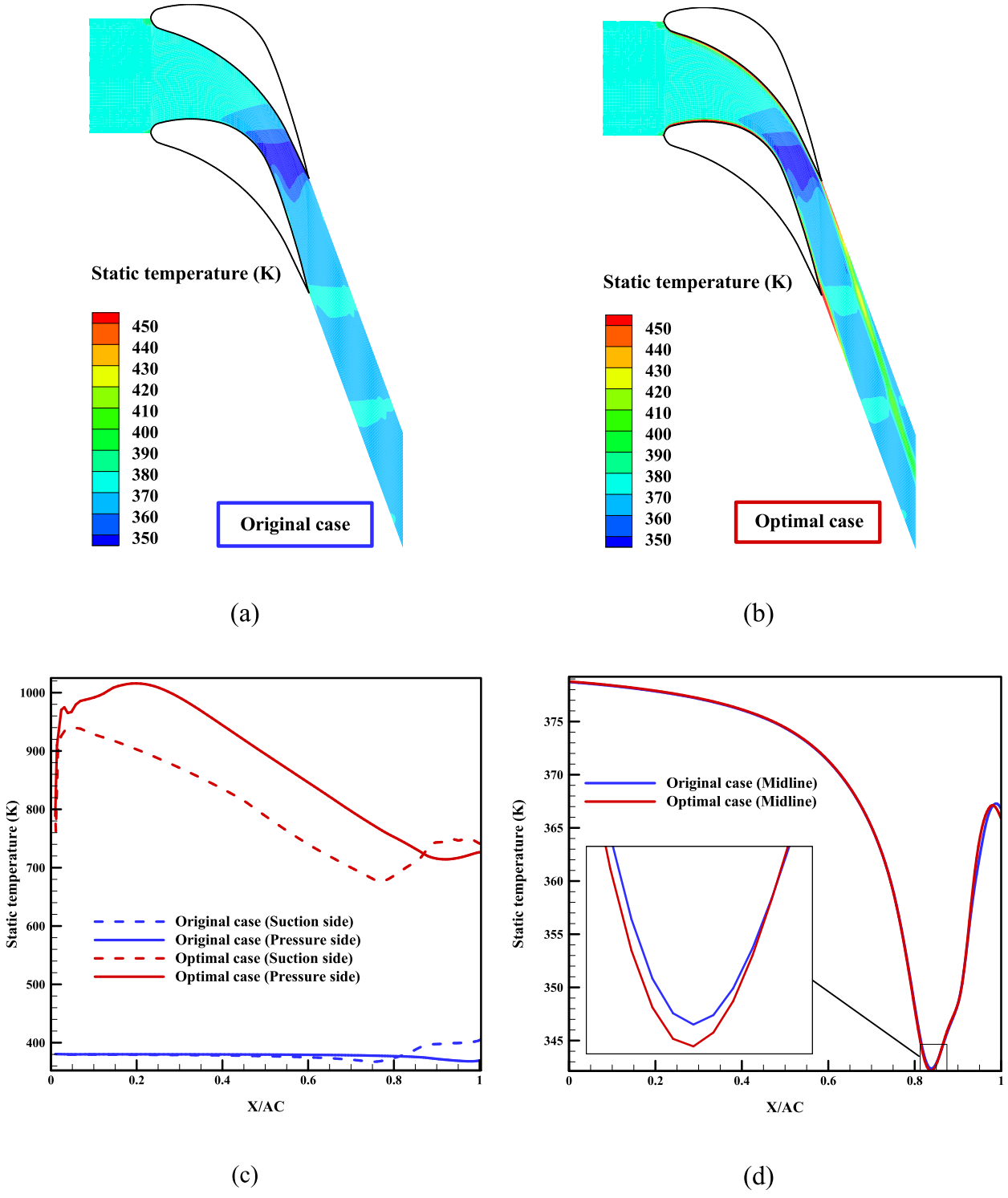


**Fig. 8.** The impacts of the surface heating on the static temperature, (a) and (b) static temperature contours of original and optimal case, respectively, (c) and (d) comparison of the static temperature on the suction side, pressure side and mid passage for original and optimal case, respectively.

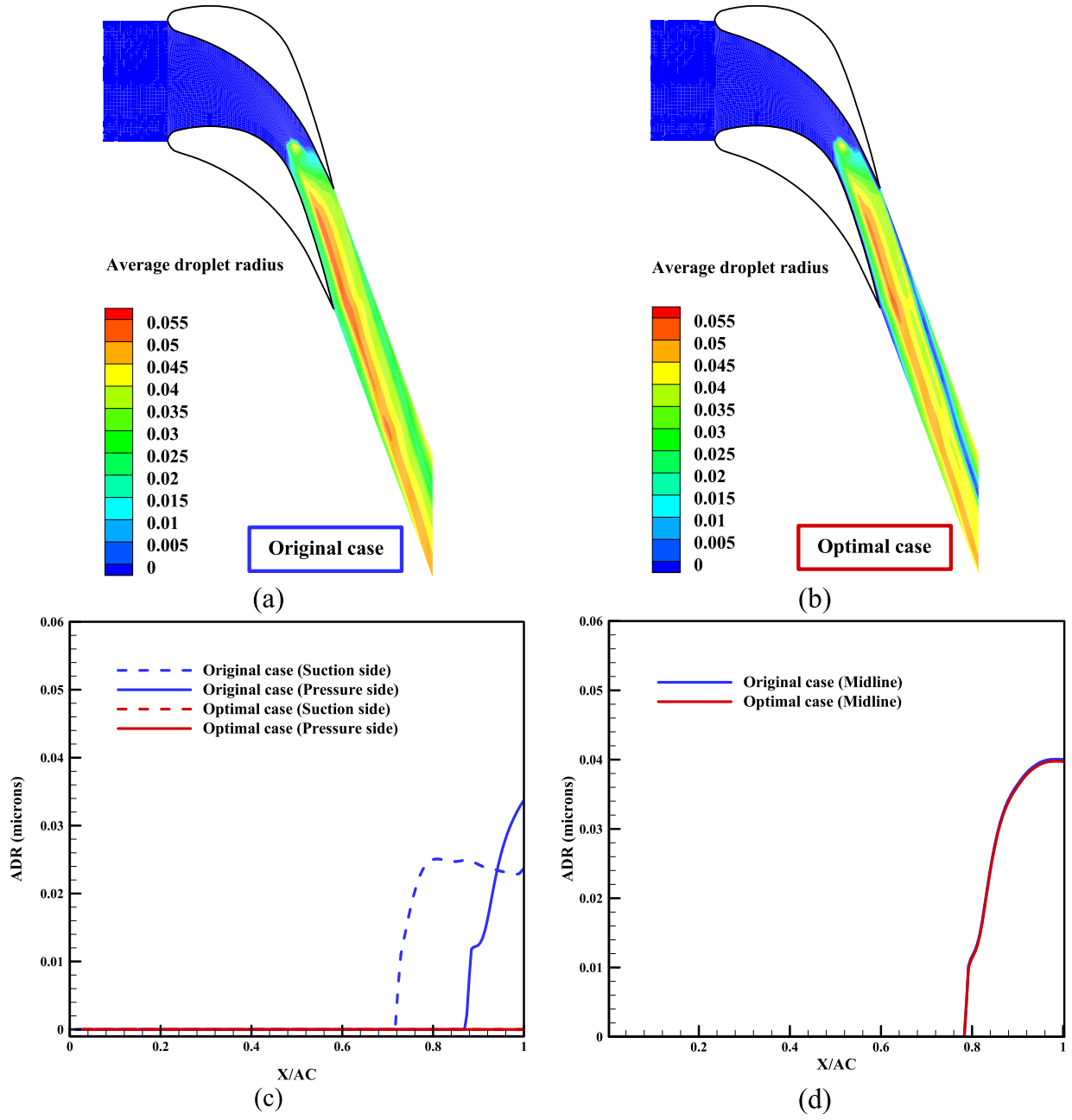


**Fig. 9.** Effects of the surface heating on the ADR (average droplet radius), (a) and (b) average droplet radius contours of original and optimal case, respectively, (c) and (d) comparison of the average droplet radius on the suction side, pressure side and mid passage for original and optimal case, respectively.

objective functions. Fig. 7 shows the Pareto frontier of MMO-NE and ILE-MWO. As shown in Fig. 7, there are three important points in the Pareto chart. In this regard, IP, NIP, and OP are ideal points, non-ideal points, and optimal points, respectively. Fig. 7-a shows pareto front of the MMO and NE. The increment of aforementioned parameters is desirable. In this regard, the IP point is obtained on the upper right side of the diagram. On the other side, the MMO and NE are in its lowest amount and therefore NIP point is not a desirable. Fig. 7-b illustrates pareto front of the MWO and ILE. The decrement of aforementioned parameters is desirable. In this regard, the IP point is obtained on the lower left side of the diagram. On the other side, the MWO and ILE are in its highest amount and therefore NIP point is not a desirable. The OP point is selected as the nearest point to the IP point. It should be noted that OP point refers to optimal surface heating [39]. Based on results, the optimal surface heating is equal to 0.04467 ($\frac{kW}{cm^2}$). Table 5 displays the variation of optimal with the original case of objective functions. As can be seen in this table, NE and MWO are improved by 0.26% and 19.94%, respectively; besides, ILE and MMO, are degraded 0.9%, 0.32%, respectively, and CP is estimated 0.0027 ($\frac{\$}{cm^2.h}$).

Fig. 9 (a-b) shows the ADR contours for the original and optimal cases, respectively. The ADR diagram is plotted on the suction wall, pressure wall (see Fig. 9-c), and midline (see Fig. 9-d) for the original and the optimal cases. By applying optimal surface heating, the average droplet radius on the mid passage is reduced, and droplets on the suction and pressure side are disappeared.

Next, the impact of surface heating on the static temperature is investigated. Fig. 8 (a, b) illustrate the contours of static temperature. Besides, the static temperature diagram is plotted on the suction wall, pressure wall (see Fig. 8-c), and on midline (see Fig. 8-d) for the original and the optimal cases. Based on Fig. 8, by adding optimal surface

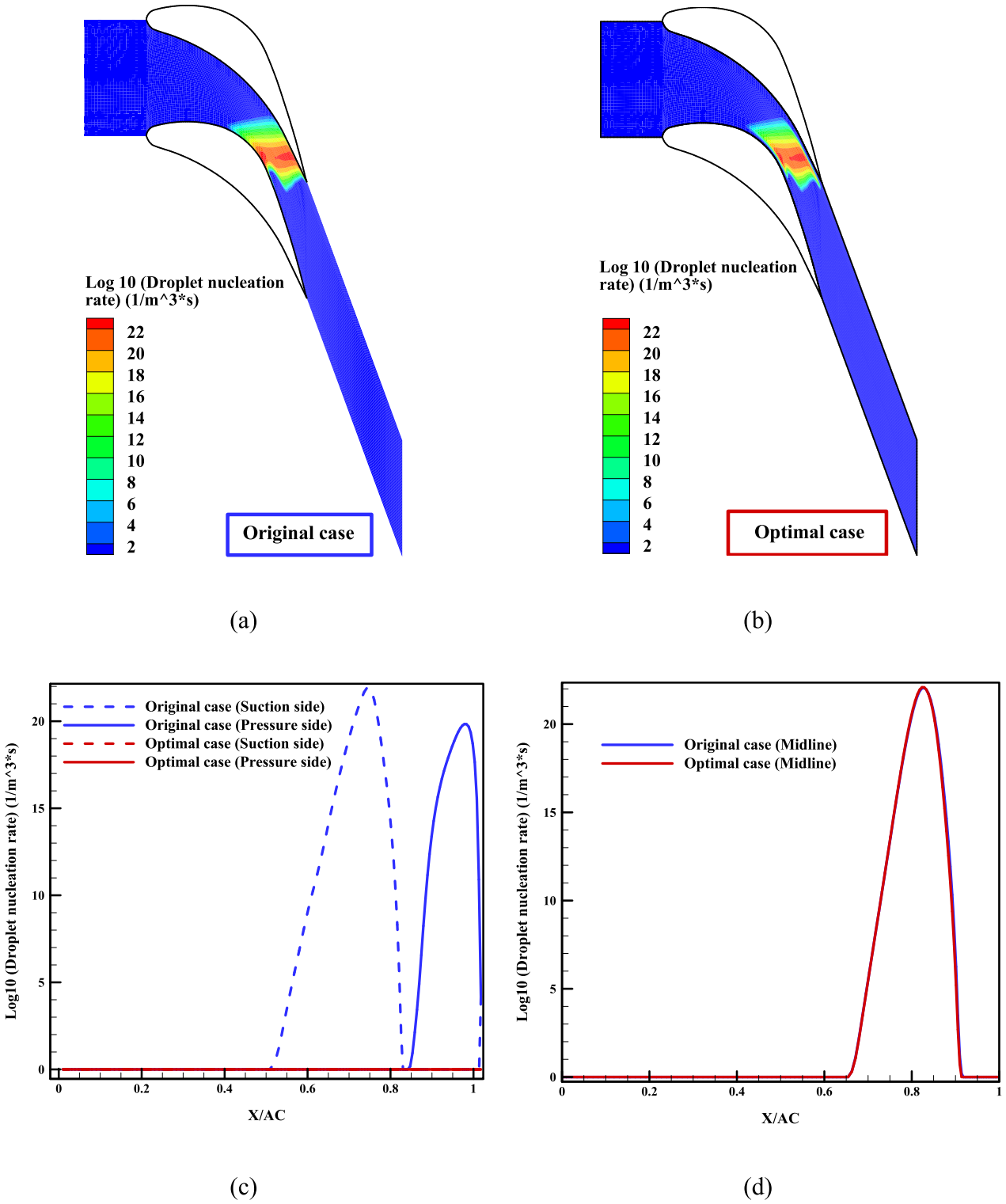


**Fig. 10.** The impacts of the surface heating on the nucleation rate, (a) and (b) droplet nucleation rate contours of original and optimal case, respectively, (c) and (d) comparison of the droplet nucleation rate on the suction side, pressure side and mid passage for original and optimal case, respectively.

heating, the static temperature of the blades is increased. It should be noted that the effect of surface heating on the centerline is negligible.

Next, the impact of surface heating on the nucleation rate is analyzed. Fig. 10 (a-b) indicates the contour of the nucleation rate. The nucleation rate diagram is plotted on the suction wall, pressure wall (see Fig. 10-c), and midline (see Fig. 10-d) for the original and the optimal cases. According to Fig. 8, by applying optimal surface heating, the blade temperature is increased; therefore, it is expected that the nucleation rate is decreased. According to Fig. 10, surface heating eliminates nucleation rate on blade surfaces.

Fig. 11 (a-b) displays the liquid mass fraction contours. The wetness fraction diagram is plotted on the suction wall, pressure wall (see Fig. 11-c), and midline (see Fig. 11-d) for the original and the optimal cases. Based on the results, by applying optimal surface heating, the

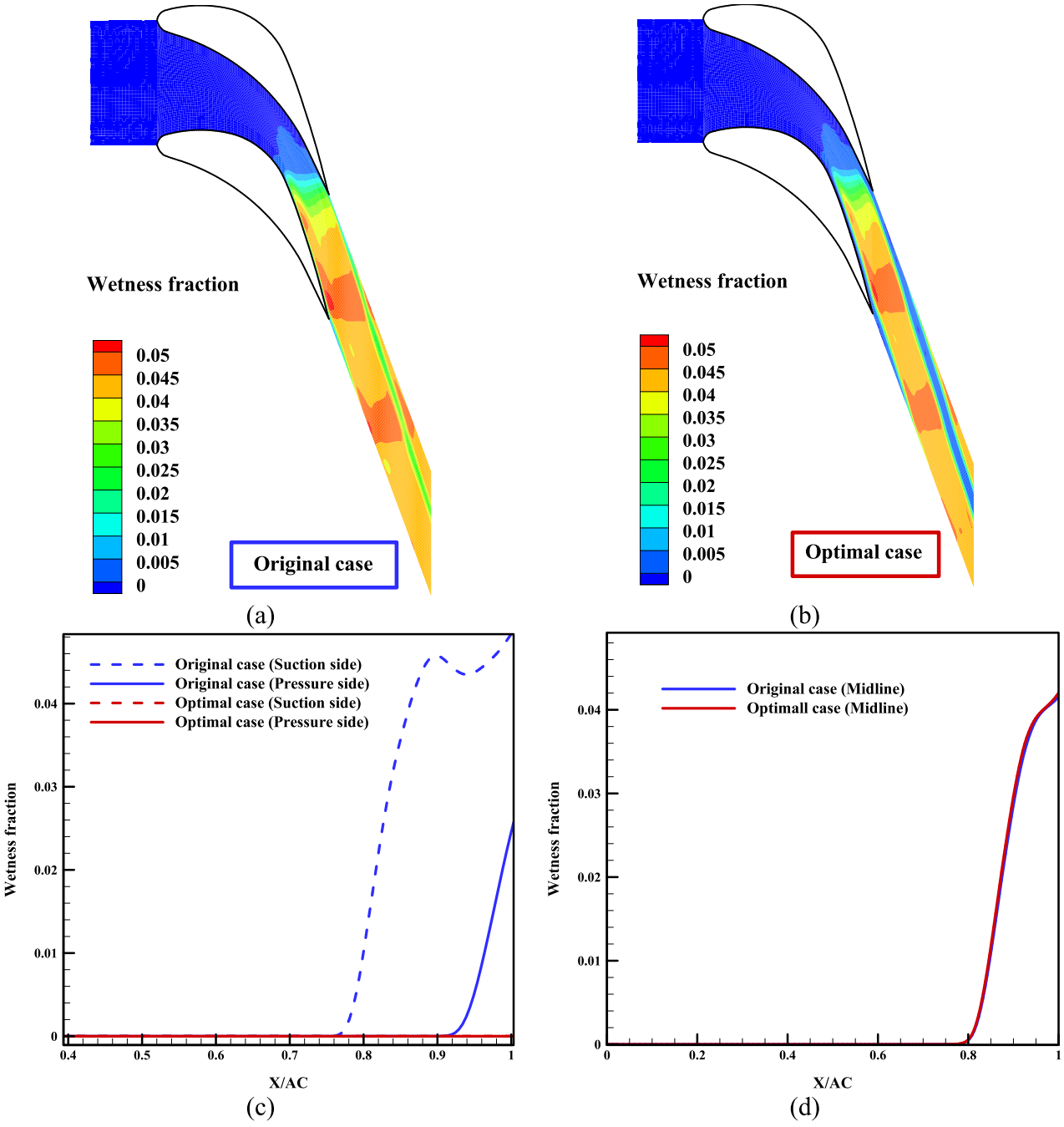


**Fig. 11.** The impacts of the surface heating on the wetness fraction, (a) and (b) wetness fraction contours of original and optimal case, respectively, (c) and (d) comparison of the wetness fraction on the suction side, pressure side and mid passage for original and optimal case, respectively.

average droplet radius on the mid-passage is reduced, and droplets on the suction and pressure side are disappeared. Besides, according to Fig. 10, by adding optimal surface heating, the nucleation on the surface blades is eliminated. In this regard, the wetness fraction on the mid-passage is diminished. The wetness fraction on the suction and pressure sides is disappeared.

Finally, the impact of surface heating on entropy is evaluated. Fig. 12 (a-b) shows the contour of entropy. Besides, the entropy diagram is plotted on the suction wall, pressure wall (see Fig. 12-c), and midline (see Fig. 12-d) for the original and the optimal cases. It is worth mentioning that applying surface heating to the flow increases the entropy of both liquid and vapor phases. As a result, by applying optimal surface heating, the entropy is increased. Based on optimization results, the optimal surface heating doesn't penetrate to midline but its effects on wall significantly. So, it is obvious that the temperature of the blade increases. On the other hand, increment of the temperature causes increase the entropy. Entropy increment is an undesirable impact of applying surface heating to the flow [20].

## 7. Conclusion

The aim of this paper is to propose the optimal surface heating for a stationary cascade turbine blade. Nozzle efficiency (NE), mean wetness at the outlet (MWO), integral of local entropy changes at the outlet (ILE), mean momentum at the outlet (MMO), and cost price (CP) are objective functions. Multi-objective optimization results show that the optimal

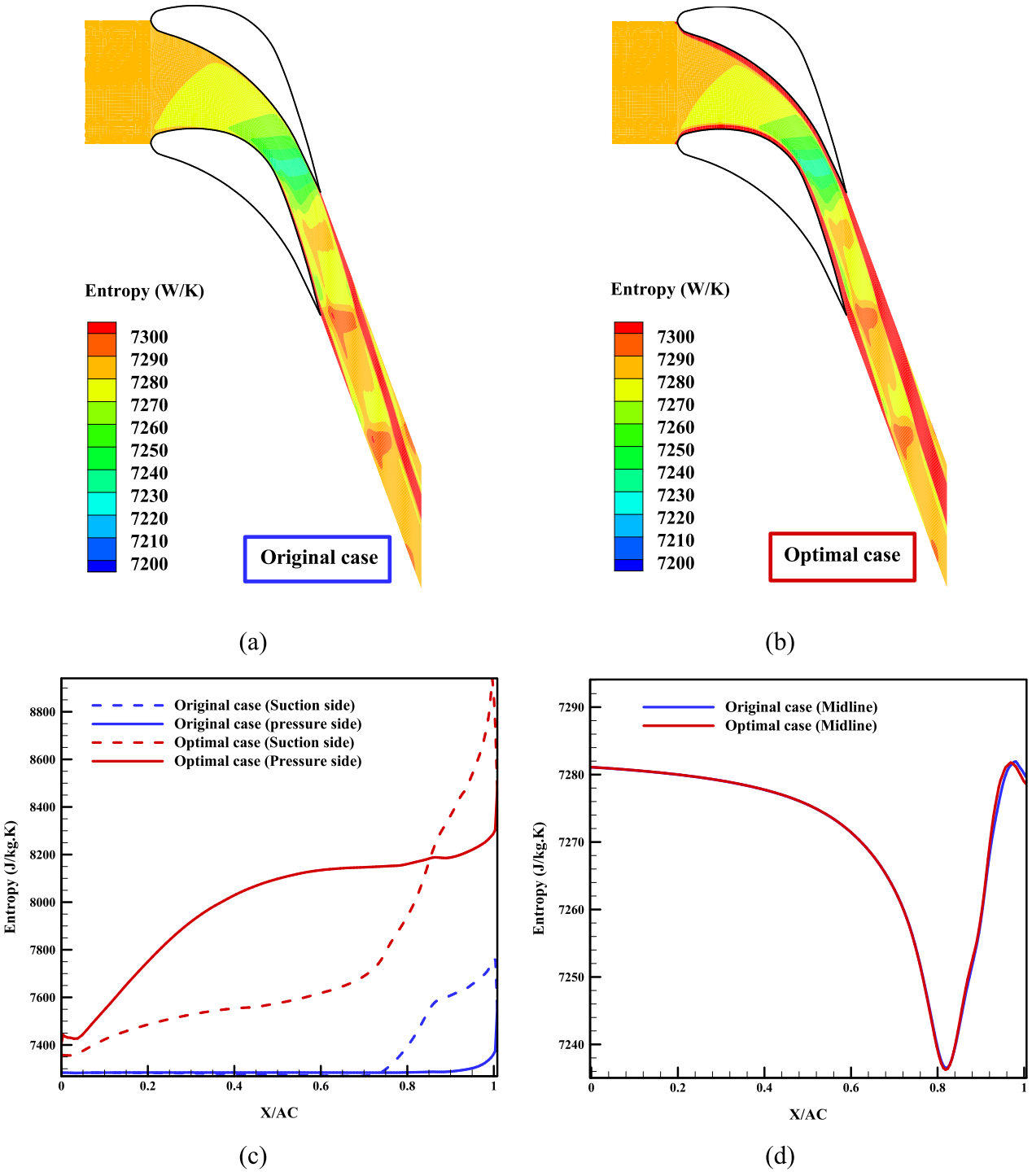


**Fig. 12.** The impacts of the surface heating on the entropy, (a) and (b) entropy contours of original and optimal case, respectively, (c) and (d) comparison of the entropy on the suction side, pressure side, and mid passage for original and optimal case, respectively.

value of surface heating is equal to 0.04467($\frac{kW}{cm^2}$). In the optimal case, compared to the non-heat case, the results are as follows:

- The nozzle efficiency (NE) and mean wetness at the outlet (MWO) are improved 0.26% and 19.94%, respectively.
- The integral of local entropy changes at the outlet (ILE), mean momentum at the outlet (MMO), are degraded 0.9%, 0.32%, respectively, and cost price (CP) is estimated 0.0027 ($\frac{\$}{cm^2.h}$).

It should be noted that by applying the proposed surface heating, erosion rate (Err) and average droplet radius (ADR) are decreased 51.15% and 10.29%, respectively.

## CRediT authorship contribution statement

**Jalal Salimi:** Validation, Investigation, Software. **Ali Reza Teymourtash:** Methodology, Writing – review & editing, Supervision. **Mohammad Reza Aghdasi:** Validation, Investigation, Software. **Esmail Lakzian:** Methodology, Writing – review & editing, Supervision.

## Declaration of Competing Interest

The authors declare that they have no known competing financial interests or personal relationships that could have appeared to influence the work reported in this paper.

## Data availability

No data was used for the research described in the article.

## Acknowledgments

This research was supported by Brain Pool program funded by the Ministry of Science and ICT through the National Research Foundation of Korea(grant number).(NRF-2022H1D3A2A02090885).

## References

[1] M.A.F. Aliabadi, A. Jahangiri, I. Khazaei, E. Lakzian, Investigating the effect of water nano-droplets injection into the convergent-divergent nozzle inlet on the wet steam flow using entropy generation analysis, Int. J. Therm. Sci. 149 (2020), 106181, https://doi.org/10.1016/j.ijthermalsci.2019.106181.
[2] A.M. Dolatabadi, F. Salmani, E. Lakzian, Analysis of Heterogeneous Nucleation and Erosion Behavior Considering the Injection of Impurities into Wet Steam Flow Using Poly-dispersed Method, Int. J. Heat Mass Transf. 185 (2022), 122392, https://doi.org/10.1016/j.ijheatmasstransfer.2021.122392.
[3] D. Dadpour, E. Lakzian, M. Gholizadeh, H. Ding, X.u. Han, Numerical modeling of droplets injection in the secondary flow of the wet steam ejector in the refrigeration cycle, Int. J. Refrig. 136 (2022) 103–113.
[4] C. Wen, X. Zhu, H. Ding, Y. Yang, Numerical Modelling of Wet Steam Flows in Turbine Blades, Adv. Heat Transf. Therm. Eng. (2021) 397–401, https://doi.org/10.1007/978-981-33-4765-6_68.
[5] P. Wiśniewski, M. Majkut, S. Dykas, K. Smołka, G. Zhang, B. Pritz, Selection of a steam condensation model for atmospheric air transonic flow prediction, Appl. Therm. Eng. 203 (2022), 117922, https://doi.org/10.1016/j.applthermaleng.2021.117922.
[6] G. Zhang, X. Wang, D. Pourranjbar, S. Dykas, H. Li, J. Chen, The comprehensive analysis of the relationship between the latent heat, entrainment ratio, and ejector performance under different superheating degree conditions considering the non-equilibrium condensation, Appl. Therm. Eng. 200 (2022), 117701, https://doi.org/10.1016/j.applthermaleng.2021.117701.
[7] C. Wen, N. Karvounis, J.H. Walther, H. Ding, Y. Yang, Effect of Turbulence Models on Steam Condensation in Transonic Flows, Adv. Heat Transf. Therm. Eng. 711–715 (2021), https://doi.org/10.1007/978-981-33-4765-6_123.
[8] G. Zhang, X. Wang, S. Dykas, M.A.F. Aliabadi, Reduction entropy generation and condensation by NaCl particle injection in wet steam supersonic nozzle, Int. J. Therm. Sci. 171 (2022), 107207, https://doi.org/10.1016/j.ijthermalsci.2021.107207.
[9] D. Walker, S. Barham, D. Giddings, G. Dimitrakis, Wet steam measurement techniques, Rev. Chem. Eng. 35 (5) (2019) 627–647, https://doi.org/10.1515/revce-2017-0078.
[10] F. Salmani, E. Amiri Rad, M.R. Mahpeykar, Investigation effects of roughness in wet steam flow with Buckingham Pi-theorem, J. Therm. Anal. Calorim. 147 (5) (2022) 3803–3813.
[11] M.R. Aghdasi, A.R. Teymourtash, E. Lakzian, Optimization of the pitch to chord ratio for a cascade turbine blade in wet steam flow, Appl. Therm. Eng. 211 (2022), 118445, https://doi.org/10.1016/j.applthermaleng.2022.118445.
[12] D. Hoseinzade, E. Lakzian, S. Dykas, "Optimization of the Trailing Edge Inclination of Wet Steam Turbine," vol. The Societ, 2021, 10.1007/s40799-021-00534-5.
[13] A. Kafaei, F. Salmani, E. Lakzian, The best angle of hot steam injection holes in the 3D steam turbine blade cascade, Int. J. Therm. Sci. 173 (2022), 107387, https://doi.org/10.1016/j.ijthermalsci.2021.107387.
[14] A.M. Dolatabadi, S. Masoumi, E. Lakzian, Optimization variables of the injection of hot-steam into the non-equilibrium condensing flow using TOPSIS method, Int. Commun. Heat Mass Transf. 129 (2021), 105674, https://doi.org/10.1016/j.icheatmasstransfer.2021.105674.
[15] A. M. Dolatabadi, E. Lakzian, M. Heydari, and A. Khan, "A Modified Model of the Suction Technique of Wetness Reducing in Wet Steam Flow Considering Power-saving," *Energy*, p. 121685, 2021, 10.1016/j.energy.2021.121685.
[16] M. Vatanmakan, E. Lakzian, M.R. Mahpeykar, Investigating the entropy generation in condensing steam flow in turbine blades with volumetric heating, Energy 147 (2018) 701–714, https://doi.org/10.1016/j.energy.2018.01.097.
[17] R. Hosseini, E. Lakzian, Optimization volumetric heating in condensing steam flow by a novel method, J. Therm. Anal. Calorim. 140 (5) (2020) 2421–2433.
[18] D. Hoseinzade, E. Lakzian, A. Hashemian, A blackbox optimization of volumetric heating rate for reducing the wetness of the steam flow through turbine blades, Energy 220 (2021), 119751, https://doi.org/10.1016/j.energy.2020.119751.
[19] X. Han, W. Zeng, Z. Han, Investigation of the comprehensive performance of turbine stator cascades with heating endwall fences, Energy 174 (2019) 1188–1199, https://doi.org/10.1016/j.energy.2019.03.038.
[20] X. Han, W. Zeng, Z. Han, Investigating the dehumidification characteristics of the low-pressure stage with blade surface heating, Appl. Therm. Eng. 164 (2020), 114538, https://doi.org/10.1016/j.applthermaleng.2019.114538.
[21] X. Han, Y. Yuan, Z. Zhao, Y. Wang, W. Zeng, Z. Han, Numerical investigation of the wet steam condensation flow characteristics in stator cascade with blade surface heating, Eng. Appl. Comput. Fluid Mech. 14 (1) (2020) 1251–1262, https://doi.org/10.1080/19942060.2020.1813631.
[22] A.J. Rahvard, E. Lakzian, F. Foroozesh, A. Khoshnevis, An applicable surface heating in a two-phase ejector refrigeration, Eur. Phys. J. Plus 137 (2) (2022).
[23] X. Han, J. Guan, Q. Zhu, and Z. Han, "Application of quadratic regression orthogonal design to optimization surface heating for control wet steam condensation flow in nozzle," *Case Stud. Therm. Eng.*, p. 101987, 2022, 10.1016/j.csite.2022.101987.
[24] F. Bakhtar, M.R. Mahpeykar,Abbas, "An Investigation of Nucleating Flows of Steam in a Cascade of Turbine Blading-Theoretical Treatment This," *j.Fluids Eng*, vol. 117, no. 1, pp. 138–144, 1995, 10.1115/1.2816803.
[25] A. Hashemian, E. Lakzian, A. Ebrahimi-Fizik, On the application of isogeometric finite volume method in numerical analysis of wet-steam flow through turbine cascades, Comput. Math. with Appl. 79 (6) (Mar. 2020) 1687–1705, https://doi.org/10.1016/j.camwa.2019.09.025.
[26] M.J. Kermani, A.G. Gerber, A general formula for the evaluation of thermodynamic and aerodynamic losses in nucleating steam flow, Int. J. Heat Mass Transf. 46 (17) (2003) 3265–3278, https://doi.org/10.1016/S0017-9310(03)00096-6.
[27] Y. Patel, G. Patel, T. Turunen-Saaresti, Influence of turbulence modelling on non-equilibrium condensing flows in nozzle and turbine cascade, Int. J. Heat Mass Transf. 88 (2015) 165–180, https://doi.org/10.1016/j.ijheatmasstransfer.2015.04.069.
[28] X.-D. Wang, J.-L. Dong, T. Wang, J.-Y. Tu, Numerical analysis of spontaneously condensing phenomena in nozzle of steam-jet vacuum pump, Vacuum 86 (7) (2012) 861–866, https://doi.org/10.1016/j.vacuum.2011.02.016.
[29] M.A.F. Aliabadi, E. Lakzian, I. Khazaei, A. Jahangiri, A comprehensive investigation of finding the best location for hot steam injection into the wet steam turbine blade cascade, Energy 190 (2020), 116397, https://doi.org/10.1016/j.energy.2019.116397.
[30] G. Zhang, F. Wang, D. Wang, T. Wu, X. Qin, Z. Jin, Numerical study of the dehumidification structure optimization based on the modified model, Energy Convers. Manag. 181 (2019) 159–177, https://doi.org/10.1016/j.enconman.2018.12.001.
[31] G.C. Benson, R. Shuttleworth, The surface energy of small nuclei, J. Chem. Phys. 19 (1) (1951) 130–131.
[32] J.B. Young, An Equation of State for Steam for Turbomachinery and Other Flow Calculations, J. Eng. Gas Turbines Power 110 (1) (Jan. 1988) 1–7, https://doi.org/10.1115/1.3240080.
[33] F.R. Menter, Two-equation eddy-viscosity turbulence models for engineering applications, AIAA J. 32 (8) (1994) 1598–1605, https://doi.org/10.2514/3.12149.
[34] S.M.A. Noori Rahim Abadi, A. Ahmadpour, S. Abadi, J.P. Meyer, CFD-based shape optimization of steam turbine blade cascade in transonic two phase flows, Appl. Therm. Eng. 112 (2017) 1575–1589, https://doi.org/10.1016/j.applthermaleng.2016.10.058.
[35] B.-E. Lee, K.-J. Riu, S.-H. Shin, S.-B. Kwon, Development of a water droplet erosion model for large steam turbine blades, KSME Int. J. 17 (1) (2003) 114–121, https://doi.org/10.1007/BF02984292.
[36] O. Ergunova, "Formation of the price mechanism for energy resources in Russia and the countries of the European union," 2018.
[37] A. Ebrahimi-Fizik, E. Lakzian, A. Hashemian, Numerical investigation of wet inflow in steam turbine cascades using NURBS-based mesh generation method, Int. Commun. Heat Mass Transf. 118 (2020), 104812, https://doi.org/10.1016/j.icheatmasstransfer.2020.104812.
[38] C. Wen, Y. Yang, H. Ding, C. Sun, Y. Yan, Wet steam flow and condensation loss in turbine blade cascades, Appl. Therm. Eng. 189 (2021), 116748, https://doi.org/10.1016/j.applthermaleng.2021.116748.
[39] A. Ebrahimi-Moghadam, S. Kowsari, F. Farhadi, M. Deymi-Dashtebayaz, Thermohydraulic sensitivity analysis and multi-objective optimization of Fe3O4/H2O nanofluid flow inside U-bend heat exchangers with longitudinal strip inserts, Appl. Therm. Eng. 164 (2020), 114518, https://doi.org/10.1016/j.applthermaleng.2019.114518.